Expandable Polymer Assisted Wearable Personalized Medicinal Platform

Wedyan Babatain, Abdurrahman Gumus, Irmandy Wicaksono, Ulrich Buttner, Nazek El-atab, Mutee Ur Rehman, Nadeem Qaiser, David Conchouso, and Muhammad Mustafa Hussain*

Conventional healthcare, thoughts of treatment, and practice of medicine largely rely on the traditional concept of one size fits all. Personalized medicine is an emerging therapeutic approach that aims to develop a therapeutic technique that provides tailor-made therapy based on everyone's individual needs by delivering the right drug at the right time with the right amount of dosage. Advancement in technologies such as wearable biosensors, point-of-care diagnostics, microfluidics, and artificial intelligence can enable the realization of effective personalized therapy. However, currently, there is a lack of a personalized minimally invasive wearable closed-loop drug delivery system that is continuous, automated, conformal to the skin, and cost-effective. Here, design, fabrication, optimization, and application of a personalized medicinal platform augmented with flexible biosensors, heaters, expandable actuator and processing units powered by a lightweight battery are shown. The platform provides precise drug delivery and preparation with spatiotemporal control over the administered dose as a response to real-time physiological changes of the individual. The system is conformal to the skin, and the drug is transdermally administered through an integrated microneedle. The developed platform is fabricated using rapid, cost-effective techniques that are independent of advanced microfabrication facilities to expand its applications to low-resource environments.

Conventional healthcare and the practice of medicine largely relies on the concept of one size fits all. This model offers the same therapeutic treatments to treat a large group of people with the same medical condition or disease. Therefore, the probability of increasing effectiveness of a treatment plan can be further enhanced. Additionally, some individuals might experience adverse effect as a result of using the general prescribed drug. Personalized medicine is a therapeutic approach that has been growing in the past few years. The aim of personalized medicine is to develop advanced patient-specific therapeutic techniques by delivering the right drug at the right time using the right amount of dosage.[1] Personalized therapy can be advantageous to regular therapy because it can provide tailor-made medications based on an individual's daily physiological changes and needs. With the advancement of technology in wearables, sensors and microfluidics devices,[2,3] all these new emerging technologies enable the realization of precision medicine and its advantages. Microfluidics drug delivery devices offer advantageous properties over

W. Babatain, Prof. A. Gumus, I. Wicaksono, U. Buttner, Dr. N. El-atab,
M. U. Rehman, Dr. N. Qaiser, Dr. D. Conchouso, Prof. M. M. Hussain
Electrical Engineering
Computer Electrical and Mathematical Sciences
and Engineering Division
King Abdullah University of Science and Technology (KAUST)
Thuwal 23955 6900, Saudi Arabia
E-mail: muhammadmustafa.hussain@kaust.edu.sa
W. Babatain, U. Buttner, Dr. N. El-atab, Dr. N. Qaiser, Dr. D. Conchouso,
Prof. M. M. Hussain
mmh Labs
Electrical Engineering
Computer Electrical Mathematical Science and Engineering Division
King Abdullah University of Science and Technology (KAUST)
Thuwal 23955-6900, Saudi Arabia

Prof. A. Gumus
Department of Electrical and Electronics Engineering
Izmir Institute of Technology
Urla, Izmir 35430, Turkey

I. Wicaksono
MIT Media Lab
Massachusetts Institute of Technology
Cambridge, MA 02139, USA

Prof. M. M. Hussain
EECS
Cory Hall
University of California Berkeley
Berkeley, CA 94720, USA

The ORCID identification number(s) for the author(s) of this article can be found under https://doi.org/10.1002/admt.202000411.

ADVANCED
SCIENCE NEWS
www.advancedsciencenews.com

ADVANCED
MATERIALS
TECHNOLOGIES
www.advmattechnol.de

conventional drug administration methods.[4] The unique fluid flow properties that emerges at the microscale can be leveraged to prepare and deliver more effective forms of drugs and therapeutics to the human body.[4] It can also be integrated with non-invasive painless administration methods through an array of skin microneedles that is seamlessly integrated into these drug delivery systems.[5] Most of existing platforms focus on single drug delivery of one type of medication or drug, as well as the delivery is an active task that has to be triggered at a specific time with a specific predetermined dose.[6–8] A drug delivery device, however, with the integration of skin sensors can provide automatic on-demand spatiotemporal control over drug preparation and release. Together, wearable devices that include sensors for continuous physiological signals monitoring as well as drug delivery components represent the next generation of customizable feedback-based personalized therapy where the patient is taking out of the loop to achieve a closed-loop smart personalized therapy. Realization of precision medicine necessitates the need for biosensors to enable the spatiotemporal control of the administered dose of drug as a response to real-time physiological changes of the patient in order to evaluate the condition of the disease and the efficacy of therapy being delivered. Advancement in soft and stretchable electronics enabled the realization of conformal bioelectronics for wearable and implantable devices with incredible functionalities.[9] Sensing elements provide information about the electrophysiological and biochemical signals of the body, actuating elements provide energy to deliver drug to the body on demand through the skin. In a further step, the sensors would collect information that assess the efficacy of the delivered drugs by continuously monitoring the changes in the physiological sign of interest. The simultaneous integration of both wearable biosensors and drug delivery devices offer a novel and a closed-loop feedback personalized medicinal platform. Here, we report a physically flexible wearable microfluidics drug delivery device for on-demand personalized closed-loop therapy. The device includes a flexible multi-reservoir microfluidics layer, flexible and conformal heating elements, skin sensors, processing and power units. The platform is able to mix different types of fluids, which with the appropriate fluid flow parameters, can be used to formulate drug micro-carriers that improve the efficacy, bioavailability and uptake of the drug in the body. Applications are not only limited to the delivery of daily multi-vitamins and minerals; the platform can also be used as more compliant alternative to conventional wearable drug delivery systems such as bulky invasive insulin pumps and wearable injectors.[10] Finally, it is to be noted, this is a proof-of-concept prototype which is not intended for any specific medical application at the moment.

Figure 1a shows a schematic illustration of the different layers composing the personalized medicinal platform. The top layer is a flexible microfluidics polydimethylsiloxane (PDMS) multi-reservoir layer. It has a thickness of 2 mm and consists of a total of 16 reservoirs with 4 different capacities to enable the storage of different drugs with different doses. The platform also has micromixers that enable the mixing capability of these different fluids on-demand upon triggering. The middle layer is a 280 μm-thick thermally expandable composite made out of PDMS and Expancel (2:1 mixture of PDMS and expandable microspheres, Expancel 031 DU 40, AkzoNobel). This layer

is spin coated on a flexible layer of heaters array. The performance of flexible heaters under different bending conditions was investigated (details found in the Supporting Information). The spatiotemporal precise infusion and delivery of multiple drugs into the skin is achieved through a painless non-invasive mechanism using stainless steel biocompatible microneedles. Figure 1d shows the integration of biocompatible stainless-steel microneedles (Micropoint Technologies) located underneath the outlet reservoir layer. The needles have a tip size of less than 1 μm providing appropriate strength for repeated skin penetrations. The height of these microneedles is around 600 μm, and because of that, it is only able to penetrate the epidermis outermost layer of the skin without causing any pain or irritation to the skin due to its continuous insertion during the usage of the devices. This also eliminates complications that usually results from the continuous use of conventional hypodermic needles for wearable applications such as skin infections. A closer look of the design of the microfluidics layer can be seen in Figure 1b, the design features a total of 16 half ellipsoid-shaped reservoirs with 4 different capacities of 295, 225, 165, and 115 μL. The reservoirs are connected to the outlet via a network of microfluidics channels with a cross section area of $150 \times 400 \ \mu m^2$ (width × depth). Another developed design with less number of reservoirs can be seen in Figure S1b (Supporting Information). Our vision for the operation of the full system includes a portable and a wearable platform as seen in Figure 1c. The portable platform includes a genome sequencing unit which will take personalization a step further. Drugs will be formulated based on the genetic make-up of each individual patient to maximize efficacy. Moreover, microfluidics technology will be used formulate those determined drugs inside effective drug carriers in order to be loaded into the personalized wearable medicinal platform patch. The whole stack is flexible enough to achieve seamless integration when assembled and worn on the body as can be seen in Figure 1d. The channels also contain individual micro-mixers as well as a final micro-mixer that is connected to the outlet. The purpose of the small micro-mixers is to prevent back flow from other reservoirs while the purpose of the main micro-mixer is to facilitate mixing of different liquids upon infusion. The geometry of the mixer is demonstrated in Figure S1 in the Supporting Information. One objective of the platform is to have mixing capabilities. Thus, it was important to understand the nature and the behavior of fluid flow inside microfluidics devices. Due to the small size of microchannels, the nature of fluid flow in microfluidics is non-turbulent laminar flow since Reynolds number is low. Reynolds number is a dimensionless number that represents the relationship between inertial forces and viscous forces[11]

$$Re = \frac{\text{Inertial forces}}{\text{Viscous forces}} = \frac{\rho v^2 L^2}{\eta v L} = \frac{\rho v L}{\eta} \tag{1}$$

In microfluidics world, the flow is always laminar due to the extremely small characteristic length (L) of the channel. Thus, mixing can be quite challenging in the microfluidics world, but it can be achieved via introducing of chaotic advection or turbulence actively active or passively by manipulating the geometry of the mixer.[12] If achieved, mixing can be utilized for many desired processes such as the synthesis of nano and micro
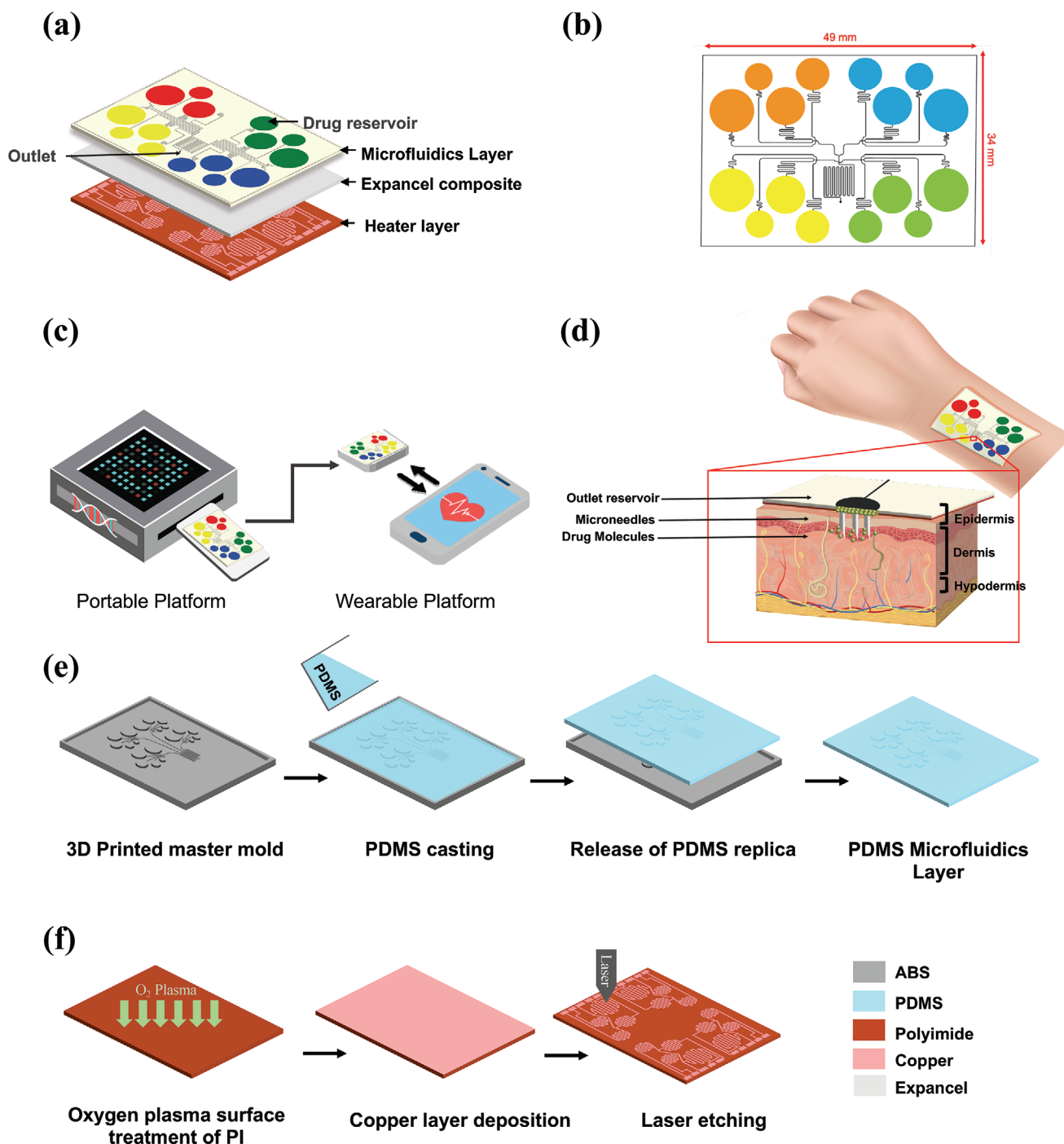
**ADVANCED
SCIENCE NEWS**

www.advancedsciencenews.com

**ADVANCED
MATERIALS
TECHNOLOGIES**

www.advmattechnol.de

Figure 1. a) Schematic illustration showing an exploded view of device. b) Design of the drug reservoirs layer congaing network of microfluidics channels and mixers. c) Conceptual demonstration of the operation of the full drug delivery system for personalized transdermal therapy. The portable device will provide optimized drug formulations enabled by genome sequencing and AI while the wearable device will provide real-time monitoring of physiological changes and actuates transdermal drug delivery accordingly. d) Schematic of microneedle integration into the device as well as the penetration of the needles though the skin layers. e,f) Process flow followed for the fabrication of the medicinal platform.

drug carriers and formulation on demand upon delivery.[13] Moreover, the platform is suitable for combinational therapy where multiple drug are being administered at the same time to achieve a desired synergetic effect.[14,15] For this application, one of the simplest passive geometry-based micro-mixers was

chosen which is composed of a semi-circular channel with a serpentine structure. In this passive type of mixer, molecular diffusion contributes to the mixing process. When two different fluids are in contact with each other, thermally induced random Brownian movements of their molecules will induce

**ADVANCED
SCIENCE NEWS**

www.advancedsciencenews.com

**ADVANCED
MATERIALS
TECHNOLOGIES**

www.advmattechnol.de

passive mixing due to diffusion. Since fluid flow in microfluidics devices is laminar, passive mixing is highly depended on molecular diffusion and advection.[16]

Diffusion of molecules occur as a result of the Brownian motion across the interfacial contacts between the fluids. Fick's law of diffusion is defined as

$$j = -D\frac{d_\varphi}{dx} \tag{2}$$

where j is the diffusion flux, D is the diffusion constant which is characteristic for a given particle, ϕ is the concentration of particles and x is the position of the particle.[16] For spherical particles, D can be defined as

$$D = \frac{kT}{6\pi\mu R} \tag{3}$$

where k is Boltzmann constant, T is the temperature, μ is the viscosity of fluid, and R is the radius of the particle. Diffusion has nonlinear relationship between the diffusion time and the distance particle travels, it is a quadratic relationship.[16,17]

Since the chosen mixer is a diffusion-based passive mixer, it was designed with one constraint which is the total length of the serpentine path. The serpentine design provides added length to the channel offering enough area and time for the two fluid streams to be in contact with each other to achieve efficient diffusion. To determine the total mixer channel length required, Einstein's equation for Brownian motion was used[12]

$$x = \sqrt{2Dt} \tag{4}$$

where, x is the average distance a diffusing particle covers within time t. In microfluidics systems, x is represented as the width of the liquid fluid that is going to be mixed along the channel. Thus, the time required to diffuse through half the channel width (W) can be calculated as

$$t = \frac{x^2}{8D} = \frac{W^2}{8D} \tag{5}$$

In this experiment, food dye is being used to carry out the mixing experiment and proof the concept. The diffusion coefficient of food coloring in water is 2×10^{-6} cm^2 s^{-1} and the width of the channel is 150 µm. Thus, the time needed for a particle to diffuse through half the channel width, W is calculated to be around 14 s. With a velocity of 37 cm s^{-1}, required length of the channel is calculated to be 52 mm to ensure complete mixing under different conditions (Figure S1c, Supporting Information). Figure 1e,f shows the process flow followed for the fabrication of the personalized medical platform. A non-lithographic inexpensive cleanroom-free approach was implemented to fabricate the microfluidics layer. For the past two decades, soft lithography has been used as the gold standard technique for fabricating or micro molding PDMS-based microfluidic devices. Although soft-lithography offers high precision technique that produces structures with high resolution, it has many disadvantages and limitations such as being a labor-intensive and costly since it requires access to

clean-room facility and is limited by the 2D layered capabilities of conventional micromachining and microfabrication processes. 3D printing on the other hand is automated, rapid, cost effective and offer greater control on producing 3D structures with incredibly complex features. In our case, the master mold design of the device was generated using a 3D computer-aided design (CAD) software and 3D printed in an ABS-like material. PDMS was then casted into the master mold and easily released to produce a fully resolved semi-circular PDMS microfluidics channels and semi-ellipsoid reservoirs. PDMS was used as the polymer of choice for its elastomeric, transparent, biocompatible and cost-effective properties. The fabrication process of the heaters array layer can be seen in Figure 1f. Method of laser-patterning was used to fabricate the electrodes of the heaters by etching the electroplated copper easily. The assembly of the different layer of the devices was achieved by using double sided adhesive film. Using this simple method of assembly as well as 3D printing enabled the Do It Yourself (DIY) approach which incredibly reduces the cost and technical knowledge required, independent of microfabrication facilities and as a result expanding the applications of microfluidics in low-resource setting and environments. **Figure 2**a,b shows optical photographs of the platform. The platform shown in Figure 2a,b can be applied and worn in different body parts when integrated with adhesive skin layer. Here, we used double sided adhesive film (30 µm thick, ARclear, Adhesive Research) to achieve the attachment. In the future, skin adhesive technology that offers a more reliable attachment be used (details found in the Supporting Information). The upper microfluidics layer is the only disposable layer in the system. After depletion of all the reservoirs on the chip, the individual can easily peel off, dispose and replace the old chip with a new filled one of loaded pre-prescribed drugs and medications (Figure S6, Supporting Information).). Figure 2b shows an example of how the platform can be seamlessly worn on the wrist (Video S1, Supporting Information). A 1 mm PDMS layer at the bottom of the platform and the side interfacing the skin is used as an encapsulation layer to prevent potential skin burn issues caused by the elevated temperature of heaters when triggered. This is layer is the orange-colored layer seen in Figure 2a, it covers the entire bottom are of the platform except the area where microneedle is present to allow direct access to skin. PDMS has a low thermal conductivity of 0.15 W m^{-1} K^{-1}, which, when combined when the thickness used, enables this encapsulation to reduce the heat transfer and prevent the high heater temperature from reaching the skin.[18]

Leveraging the inexpensive rapid fabrication techniques used, the design of the device can be modified and tailor-made for each individual based on their medical conditions and therapeutic requirements. The expandable polymer used as the pumping actuator in this device is composed of a mixture of PDMS and Expancel microspheres. Expancel undergoes a rapid and irreversible volumetric expansion around 7 times more of its original volume upon heating it to around ≈80 °C. Adding mixing capability to the platform is a first step to enable formulation and preparation of drug microcarriers in the future. For demonstration and proof of concept purposes, food dye colored water solutions were used and filled up the reservoirs. By selectively triggering different drug reservoirs of the platform, the desired fluids were ejected out of the device as seen
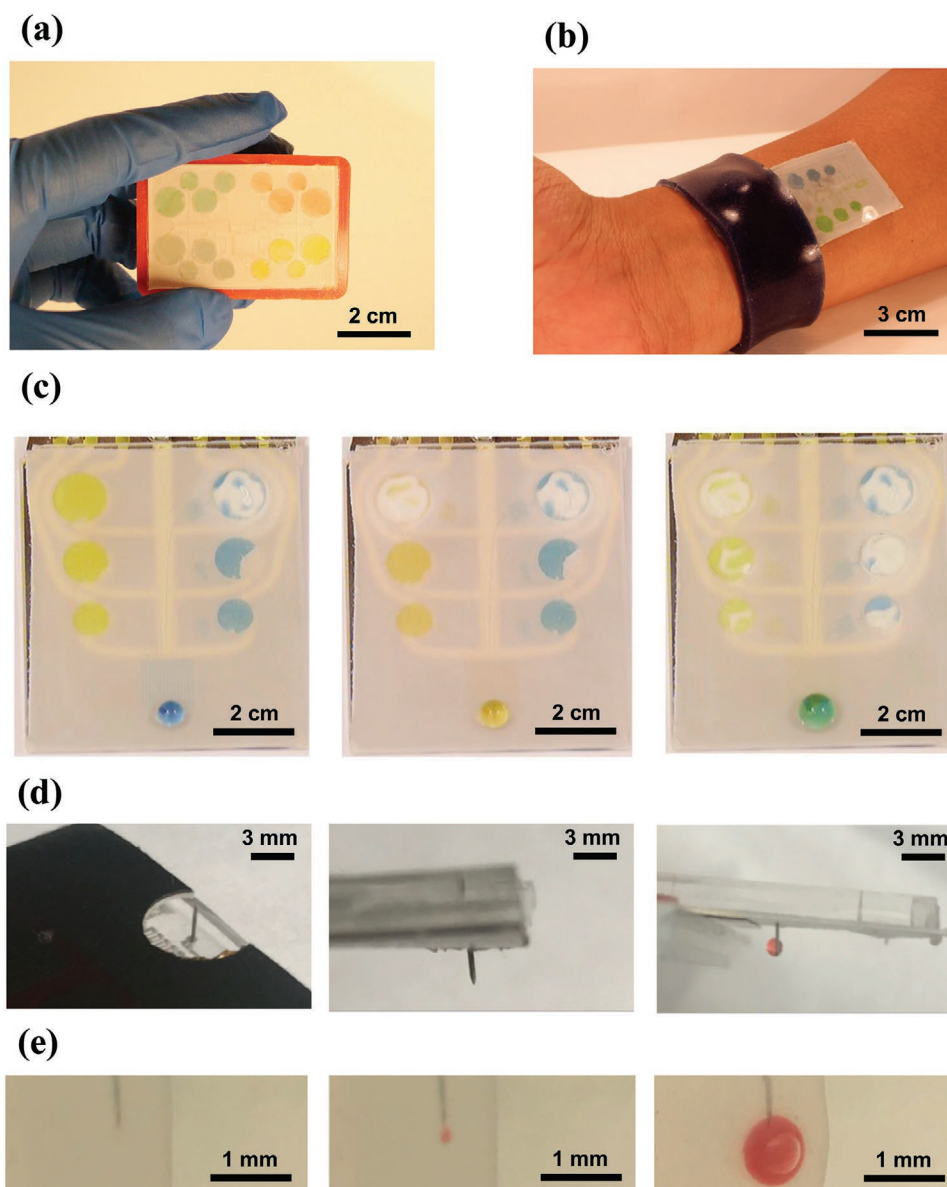
Figure 2. a) Photograph of the microfluidics layer after filling and sealing the reservoirs. b) The platform applied on a wrist. c) Validation of microfluidic mixing capability of the platform where blue and yellow liquids yield a green colored liquid at the outlet. d) Optical photographs of the microneedle integrated into the platform. On the left, the integration of the miconeedle underneath the outlet is shown. On the tight, the infusion of the fluid through the microneedles is shown. e) Sequence of photographs showing the successful insertion of microneedle into the phantom skin as well as liquid infusion.

in left image of Figure 2c. Initially, reservoirs containing blue and yellow colored water were triggered separately and then both reservoirs where triggered simultaneously and fluid were ejecting and mixed (blue and yellow) upon the passage through the mixer to form a desired mixture output (green) at the outlet as can be seen in right image of Figure 2c. Upon reaching the micromixer, successful mixing of fluids occurs, and the infusion occur via the microneedles located underneath the outlet reservoir. To assess the fluid release through the microneedle, a layer of Ecoflex 00-30 silicone elastomer was used to mimic the skin. Figure 2d shows optical photographs of the microneedle when integrated into the platform and Figure 2e shows the successful penetration of the microneedle into the skin mimicking

layer as well as the successful infusion of liquid into the layer. Ecoflex is a silicone elastomer that is a good candidate to achieve the goal of this demonstration. Ecoflex has Young's modulus of 125 kPa that is closely similar to that of the human skin and has been used widely in such applications.[19,20] Silicone rubber phantom skin has been used previously specifically to characterize needle insertions for soft tissues due to its similar mechanical properties of the human skin.[21,22] In the future, we plan to investigate the platform and microneedle performance when applied to porcine skin in vitro.

Figure 3a shows the temperature rise over time after triggering the heater. It can be seen that initially the heater experiences a rapid temperature rise reaching the critical temperature
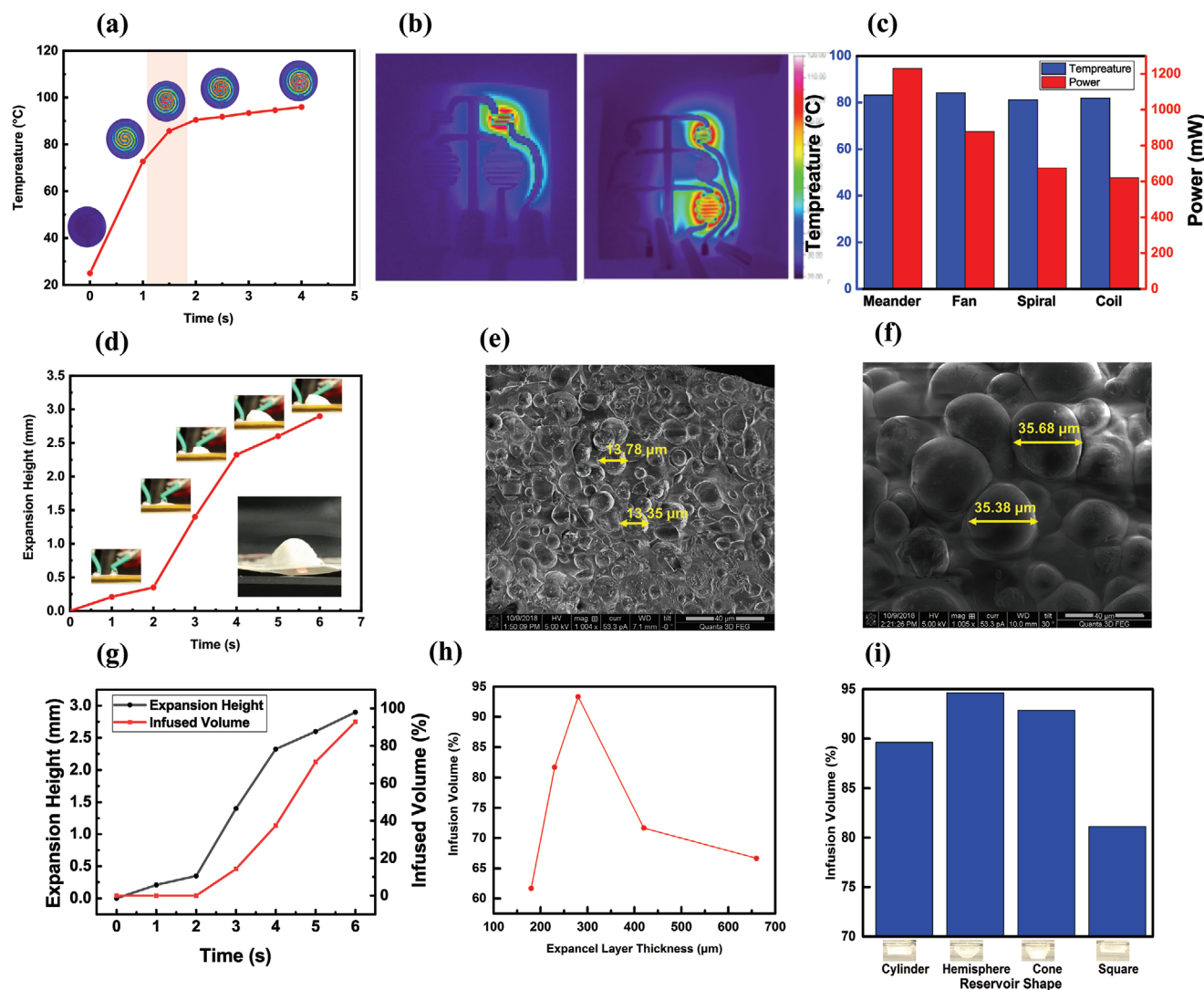
Figure 3. a) Experimental results of temperature increase upon triggering the heater showing a period of 1.5 s needed to reach the critical temperature of >80 °C. b,c)Thermal characterization of microheaters. Infrared (IR) thermal images of powering of single heater (left) and multiple heaters at simultaneously (right). c) Thermal analysis of different microheater patterns. d) Evolution of the height of the expansion profile of the composite after initial triggering inset shows a photograph of the sideview of the expansion profile of the composite. e,f) SEM image of expancel microspheres e) unexpanded and f) fully expanded microspheres. The scale bar value is 40 µm. g) Percentage of the fluid infused volume as a function of time and expansion profile height. h) Fluid infusion volume as a function of thickness variation of expancel composite. i) Fluid infusion volume as function of the reservoir shape/geometry.

of >80 °C after 1.5 s only while Figure 3b shows IR thermal images that show the capability of the device in triggering single reservoir at a time or simultaneous triggering of multiple reservoir as needed. The distance between heaters and corresponding reservoirs was designed to be at least 2 mm to prevent any unintentional triggering of neighboring reservoirs (details found in the Supporting Information). The shown isolated Joule heating for each heater confirming the functionality of the design. Since the device is a wearable device, power consumption is a crucial parameter that had to be considered. The heating element relies on the principle of Joule heating where an electric current is passes through a conducting element to produce heat. The goal was to investigate different patterns of electrode and to choose the one that will provide the required critical

temperature of 80 °C while consuming the least amount of power. In order to optimize the design of the heater being used, different heater electrode designs were fabricated and tested (Figure S2, Supporting Information). Designs used were the meander structure, the fan structure and the spiral structure. The rise in temperature and mapping of the heating profile was captured using infrared thermal imaging camera as can be seen in Figure 3c. The Figure shows the amount of power each electrode design consumes when the maximum temperature is close to the critical temperature of around 80 °C. Based on power consumption, the coil spiral design was found to consume the least amount of power compared to the meander and fan designs. Thus, the spiral pattern was selected as the optimal design to be used for the micro-heaters in this device. In order

**ADVANCED
SCIENCE NEWS**

www.advancedsciencenews.com

**ADVANCED
MATERIALS
TECHNOLOGIES**

www.advmattechnol.de

to investigate the reasoning behind why the spiral design performed better than the others, one needed to take a closer at the effect of the geometrical elements present in each shape. One critical geometrical element is the number of corners or sharp edges the pattern contains. Sharp corners cause electron accumulation and current crowding. This electron accumulation leads to the generation of micro-cracking, electro-migration failure, and localized heat rise which all result in a shorter lifetime of the heater and lowers the maximum temperature it can reach. The results of several studies that investigated the performance of different heater geometries confirm the results found here.[23,24] Thus, minimizing the number of corners and having rounded coroners was reported to yield better power efficiency as the electron accumulation is reduced, the localized temperature rise is reduced resulting in an overall increase in the maximum temperature reached by the heater.[23,24] Hence, the coil pattern resulted in less power consumption because of the absence of sharp corners and edges and minimization of heat losses. The temperature increase of to the critical temperature of >80 °C introduces a potential concern regarding temperature elevation of the fluid inside the reservoir. We have monitored the temperature of the upper layer when it expands, which in direct contact with the fluid. IR thermal image in Figure S9a in the Supporting Information shows the temperature profile of the bare heater layer on the 5th second of activation, where it reaches the critical temperature of >80 °C. Figure S9b in the Supporting Information, however, shows the temperature profile when the upper Expancel layer is assembled on top of the heater. It can be seen that the maximum temperature that layer reaches on the 5th second of activation is in the range of 50–60 °C. This temperature profile of the upper layer that is in direct contact with the fluid implies that the temperature of the fluid in the reservoir will be equal or less than the range of 50–60 °C. This range of fluid temperature is compatible with some pharmaceutical drugs that were reported to remain stable and maintain their chemistry even after storage in an elevated temperature setting of 50–60 °C.[25,26] It is also important to note here that this rise in temperature happens for a very short period of time of 5 s and decreases rapidly afterward, which is less likely to cause any concern regarding drug degradation due to that instantaneous increase in temperature. Moreover, a study conducted by Jeong et al. reported that the result of a simulated fluid dynamic model of a microfluidic probe with a comparable channel length showed that the rapid elevation in fluid temperature decreases incredibly as it travels through the channel such that by the time it reaches the outlet, the temperature rise in the fluid is less than 0.1 °C which is not significant.[8] This indicates that there will be no issue regarding drug elevated temperature when it is penetrating the targeted tissue of delivery. It is critical to mention that not all pharmaceutical drugs will be compatible with this drug delivery platform. If the active drug compound exhibits degradation or decomposition at trainset heating of about 50–60 °C for 5 s, it may not be optimal to use it within this platform. It is imperative that specific testing is performed prior to the use of such drugs in order to confirm their compatibility with the system.

The inset in Figure 3d shows a side view of the composite expansion profile upon reaching the required critical temperature. This expansion pumps the fluid out of the triggered

reservoir into the channel. Figure 3d shows the evolution of the expansion profile height with time after the initial triggering the heater. It can be seen that sufficient expansion with height of around 2.7 mm is reached on the 5th second. This height is enough to cover a reservoir with a 3 mm thickness. The results in graph 3h confirms this conclusion as it shows that the volume of fluid being infused reaches it maximum of 93% at the 5th second too. Moreover, it shows the linear correspondence between the two factors of expansion height and amount of infused volume. Figure 3e,f shows SEM images of Expancel microspheres before and after heater activation. It can be seen that on average, the microspheres experienced enlargement of up to two and a half times its original size. Figure 3g shows the amount of fluid being infused as the expansion height increases causing the depletion of reservoir. Almost complete depletion occurs at the 6th second. Here, the total height of the reservoir was fabricated to be 3 mm. The thickness of the PDMS-Expancel composite is an important parameter that affect both the expansion ratio as well as the amount of fluid being infused from the reservoir. The goal is to deplete the reservoir completely in order to deliver the prices amount of the defined desired dosage. Thus, the optimum thickness of PDMS-Expancel composite layer was investigated by altering the spin coating speed during fabrication. Figure 3h shows the different thicknesses of PDMS-Expancel composite that were used and the corresponding amount of fluid volume that was infused as a percentage from the original amount of fluid in the reservoir. The experiment showed that the optimal thickness of PDMS-Expancel composite is 280 µm, which infuses 93.33% of the total volume of the reservoir. It can be seen from Figure 3h that the relationship between the thickness of expancel layer and the infusion volume starts as an almost linear relationship which is expected. The thicker the layer is, the more expancel microspheres are there ready to expand and as a result the total effect of expansion of each is reflected in an overall larger expansion profile. Higher volume expansion corresponds to the ability of the expanded layer to cover majority of the reservoir volume and thus displacing most of the fluid out of the reservoir. Beyond 280 µm, however, it was observed that as the thickness of expancel layer increases, the amount of fluid being infused decreases. This can be explained by looking at the thermodynamic behavior of Expancel and its properties in the expanded state. Expancel microspheres in their expended state act as good thermal insulating units. This is because when it is expanded, the gas-filled voids in the composite and the phase change decreases the thermal conductivity of the overall composite from 0.2 to 0.06 W m^{-1} K^{-1}.[27] It is reported that this thermal insulation capabilities can be observed with layers of thickness of around 1.0–1.5 mm for optimal thermal insulation performance.[27] From Figure 3h, it can be noticed that as Expancel layer becomes thicker, the amount of fluid infused decreases which implies that Expancel layer did not provide sufficient expansion to deplete the reservoir. This indicates that at thickness above 280 µm, expansion of Expancel is slowed down as the expanded microspheres that located close to the heater are now acting as thermal insulating layer for the upper unexpanded microspheres.[28] This will overall halt the expansion and decreases it. Thus, the behavior of Expancel composite can be divided into two main regions. The first region is when the

ADVANCED
SCIENCE NEWS
www.advancedsciencenews.com

ADVANCED
MATERIALS
TECHNOLOGIES
www.advmattechnol.de

overall expansion is limited by the number of microspheres that exist, which representative in the thickness of the composite. This can be considered as the ideal thermodynamic expansion behavior of Expancel. In this region, thickness of the composite layer and the amount of fluid being infused is almost linear. In the second region which lies beyond the thickness of 280 μm, the overall expansion is limited by the heat transfer as the already expanded Expancel layer acts as thermal insulating unit which makes it difficult for heat to be conducted and reach the upper unexpanded part of the layer. This decline of expansion leads to an overall expansion height that is less than the ideal expanded height, which results in less volume being displaced from the reservoir. Another important parameter that affect the volume of fluid infused is the shape of the fluidic reservoir. Different shapes of reservoir were fabricated and tested including a cylinder, a hemisphere, a square, and a truncated cone reservoir. The results in graph 3i indicate that the hemispherical type of reservoir infused the highest volume of liquid with a percentage of ≈95% of the original reservoir volume. This result can be explained by looking at the molecular shape of Expancel. Expancel consist of tiny microspheres that contain liquid hydrocarbon encapsulated inside a thermoplastic shell. When heated, the thermoplastic shell softens and the enclosed hydrocarbon changes phase from liquid to gas and results in expansion. Upon expansion, the microspheres still maintain their spherical shape and the overall expansion profile of the composite forms an almost hemispherical shape that can see in the inset of Figure 3d. This expansion profile conforms the most to the hemispherical reservoirs, and as a result it depletes most of the liquid out of the reservoir more efficiently than the other shapes. In order to study the effect of channel size and shape on mixing efficiency, COMSOL MultiPhysics simulation of the micromixer with the defined calculated geometry was performed (**Figure 4**a–e). The first parameter that was studied and optimized was the depth of the channel. COMSOL simulation has been made by varying the depth of the channel using depths of 100, 200, 300, and 400 μm while fixing the width to 100 μm. Two fluid of concentrations of 0 and 1 mol m^{-3} were used in the analysis as well as 0 1n 100 mol m^{-3}. Figure 4a shows the graphical representation of mixing results obtained through COMSOL simulation for varying depth. Here, the unit number represents every turn in the serpentine structure. It can be seen that deeper channel results in rapid and efficient mixing as it allows for increased contact area between the two fluids facilitating diffusion.[29] Another parameter that was optimized to improve mixing was the cross-section shape of microchannel compromising the mixer. Two channel geometries were studied, a circular and rectangular -based channels (Figure S7b,c, Supporting Information). Square-shaped microchannels are more common due to their ease of fabrication using common soft lithography and micromachining process. Circular and rounded- shaped microchannel, are common in large-scale fluidic system, but are not common in microfluidics because of their complex fabrication process. With the advancement in rapid prototyping techniques such as 3D printing and was adopted in this project, these structure can be easily fabricated nowadays.[30] Figure 4b shows a graphical representation of mixing results obtained through COMSOL simulation for varying the shape of the channel, the total volume of the mixer

was fixed for both shapes. It can be clearly observed that circular channel provided better mixing than the rectangular microchannel mixer since the complete mixing reaching a concentration of 50 mol m^{-3} was reached at a lower unit number than the rectangular channel-based mixer. This result has also confirms with what has been reported in other studies such as the one reported by Balasubramaniam et al.[31] The study has shown that channels with circular cross sectional profile affect the strength of the produced Dean vortices which enhances the diffusion process of mixing.[31] Figure 4e,f shows the corresponding simulation results (e) design and concentration profiles of the rectangular-shaped microchannel mixer and (f) design and concentration profiles of the circular-shaped microchannel mixer, along the mixers units. Since the goal is for the platform to enable mixing, it was important to study the capability of the mixer of mixing fluids of various viscosities. Figure 4c demonstrates the performance of the mixer in mixing fluids of similar viscosities, i.e., water (viscosity of 1 cP) with water (viscosity of 1 cP) and mixing fluids of different viscosities, i.e., glycerol 60% (v/v; viscosity of 10.8 cP) with water (viscosity of 1 cP).[32] In order to evaluate the efficiency of mixing, the following equations that were previously published in the literature were used.[18,19] Mixing efficiency was measured by

$$\sigma = 1 - \sqrt{\frac{1}{N}\sum_{i}^{N}(\sigma_i)^2} \qquad (6)$$

where σ_i is the total deviation at pixel i

$$\sigma_i = \frac{(I_i - I_{mix})}{(I_{unmix} - I_{mix})} \qquad (7)$$

σ_i is the intensity of the images at pixel i, I_i is the intensity of the mixing picture, I_{unmix} is intensity prior to mixing, and I_{mix} is the intensity after complete mixing.

ImageJ processing software was used to acquire color intensities inside the microchannel and plugged into Equation (6) and (7). The mixing index corresponds to the degree of mixing, 0 for unmixed state and 1 for completely mixed state. It can be seen from Figure 4c that the platform provided mixing efficiency of 100% at the end of sixth unit when mixing colored water with same viscosity and mixing efficiency of about 65% when mixing fluid of 1 and 10.8 cP viscosities. In order to expand the application of the platform for liquids of various viscosities and improve efficiency of the mixer beyond 10.8 cP, we have modified the design of the mixer, specifically increased the total overall length of the mixer by adding six extra meandering units. The presence of longer mixing path increases the diffusivity of the solutes in fluids of different viscosities since it offered longer area and time for the two fluid streams to be in contact with each other to achieve efficient diffusion. As seen in Figure 4f, the platform provided a mixing efficiency of about 95% when mixing fluid of 1 cP (water) and 22.5 cP (glycerol 70%). This new improvement on the design of the mixer enabled efficient mixing of higher viscous fluids; as a result, expanding the range of liquids to be used within the platform. It has been shown that mixing enhancement is achieved by modifying the design of the original mixer. In the future, more advanced designs can be introduced to the
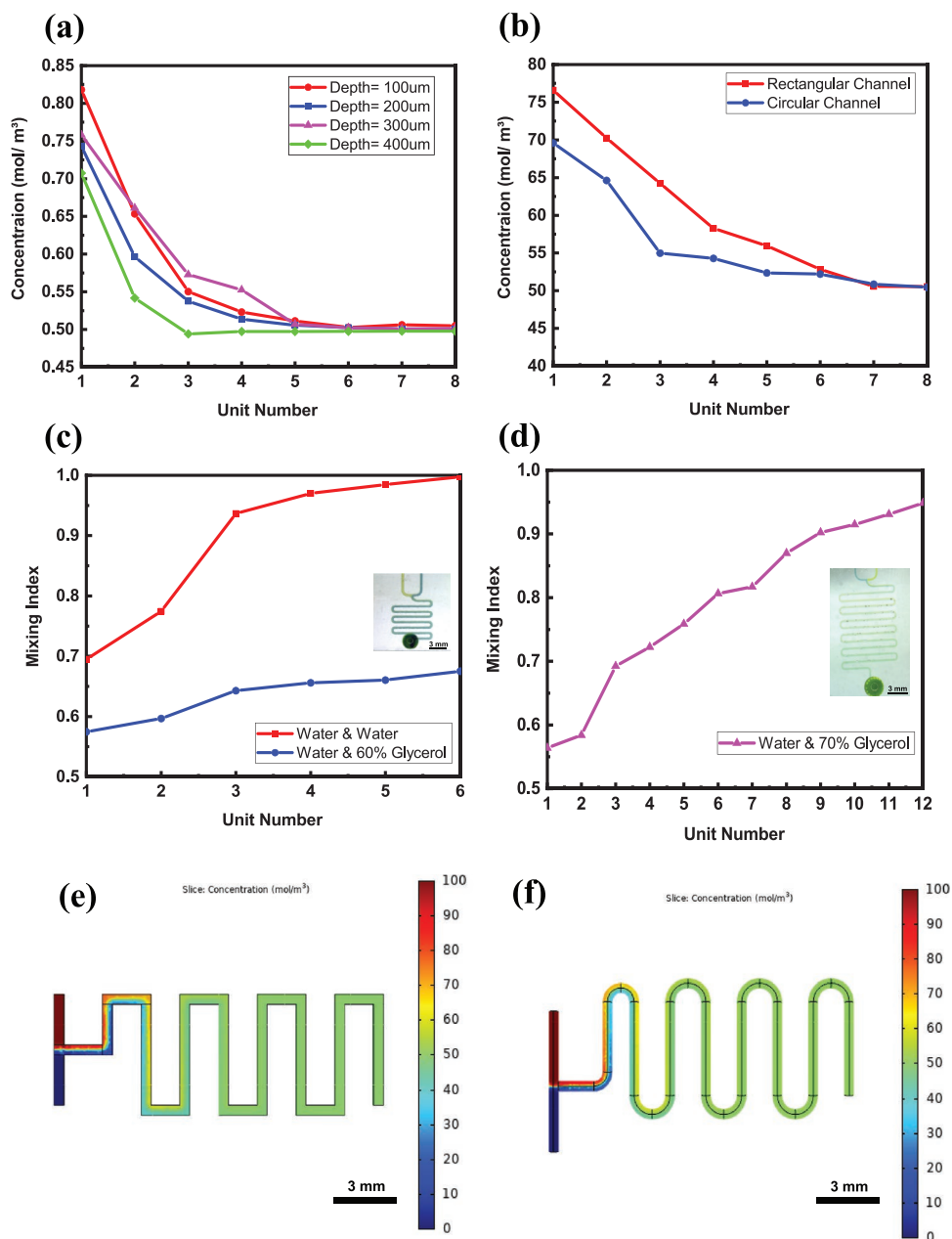
2000411 (8 of 12)

Figure 4. a) Concentration profile along the mixer units when mixing fluid of 0 and 1 mol m^{-3} for channels of different depths. b) Concentration profile along the mixer units when mixing fluid of 0 and 100 mol m^{-3} for channels of different cross sectional. c) Mixing index versus the mixer unit number when mixing fluid of similar viscosities and fluids of different viscosities. The inset shows a photograph of mixing experiment when mixing aqueous solutions of similar viscosity, the value of inset scale bar is 3 mm. d) Mixing index versus the mixer unit number when mixing water and fluid glycerol 70% solution. The inset shows a photograph of mixing experiment when mixing water fluid and glycerol 70% solution, the value of inset scale bar is 3 mm. e) Mixing simulation results of a rectangular-shaped channel. f) Mixing simulation results of a circular-shaped channel.

platform, such as the addition of 3D and groove structures, which will offer significant mixing performance enhancement for higher viscosity fluids.[33] It is important to note that microfluidics devices fabricated using 3D printed technology produce increased surface roughness compared to devices fabricated using standard soft lithography techniques.[30] The roughness of the 3D printed reliably transferred to the resulting PDMS casted device. Figure S8 in the Supporting Information compares the surface roughness measurement of PDMS device

casted using PMMA molding 3D printed molding. The general RMS surface roughness was 196 and 0.819 nm for 3D printed part-molded and PMMA-molded devices respectively. Although increased surface roughness can be considered as a limitation in some situations, it is considered advantageous for mixing purposes. It has been reported in previous studies that the presence of increased roughness on the surface creates local oscillations and vortices which induces turbulence and improves diffusive mixing.[34]
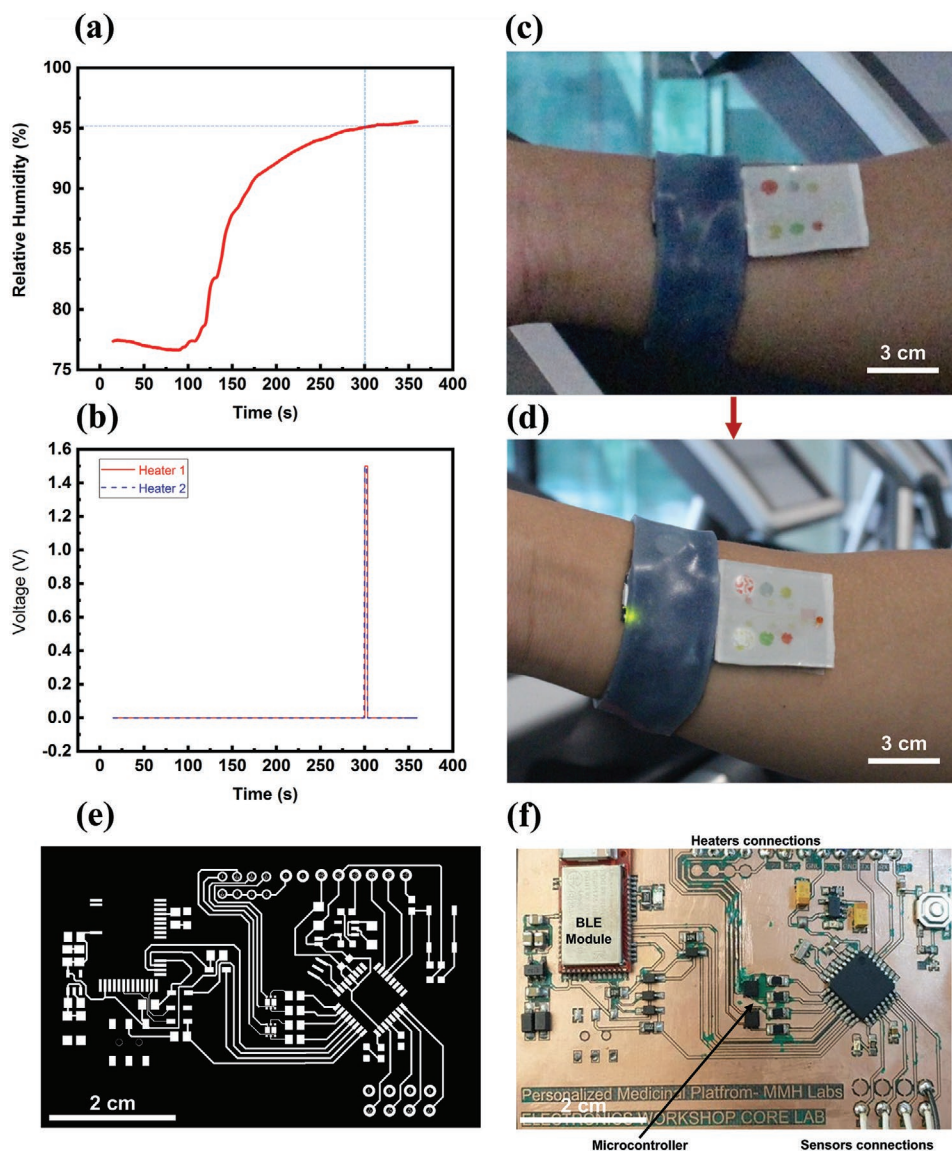
**ADVANCED
SCIENCE NEWS**

www.advancedsciencenews.com

**ADVANCED
MATERIALS
TECHNOLOGIES**

www.advmattechnol.de

Figure 5. a–d) Closed-loop feedback experiment: a,b) triggering the device after detecting physical fatigue from wearable sensors. c) The platform before and d) after actuation. e) Layout of the of the printed circuit board including the microcontroller and BLE. f) Optical image of the PCB after soldering the required components.

In order to demonstrate the application of the integrated system in a closed-loop feedback autonomous manner, the platform was placed on the wrist of a subject during physical exercise. After real-time detection of physical fatigue from wearable sensors, the corresponding programmed reservoirs were triggered to release the fluid (Video S2, Supporting Information). **Figure 5**a shows the percentage of relative humidity over time. Once the programmed threshold of 95% relative humidity was reached, instant triggering of both heaters was initiated. As a result, the fluid was ejected from both reservoirs and mixed before reaching the outlet as seen in Figure 5c,d. It is important to note here that in this experiment, and for proof of concept purpose, only the humidity and temperature sensors were used. In the future, more biosensors will be incorporated in order to provide a more accurate assessment of the physiological state of the human body. Figure 5e illustrates the

layout of the flexiable printed circuit board (PCB), for both the microcontroller unit and the Bluetooth low energy (BLE) unit. In Figure 5f, an optical photograph shows the flexible PCB after soldering the required components such as microcontroller and BLE. The PCB is the integrated with heater, current driver circuitry flexible humidity and temperature sensors. The PCB is fabricated on a flexible substrate which provide the needed conformity for such wearable device to be fully functional and comfortable for long periods of use.

In this project, we have shown a wearable transdermal drug delivery platform that is aimed to pursue the goal of on-demand personalized medicine. The platform successfully demonstrated fluid mixing and delivery on demand using an expandable composite as the main pumping mechanism to displace fluid from pre-defined reservoirs upon triggering heating elements underneath the expandable composite. Although

expancel composite have been used previously by other groups to actuate microfluidics devices, this study presented extensive optimization of important parameters in order to maximize the performance of expancel as a drug delivery pump. Rapid inexpensive fabrication approaches such as 3D printing and laser micromachining were utilized in the fabrication process of the platform to reduce cost and enable its large-scale use. We have also shown the integration of wearable sensors that are continuously collecting physiological signals from the body in order to provide autonomous closed-loop therapeutic actions. This feedback function will be the next paradigm shift for healthcare in the future. Effort is needed in the future with regard to the development and packaging of the platform to enhance its stability, reliability, and long-term use. In the future, the microneedles that were used for transdermal delivery can also be used for biosensing purposes. The same pump can be designed to work in a reverse manner to draw or collect bodily fluid like sweat which carries many important metabolites and analytes. Moreover, sensors and artificial intelligence algorithms can be used to assess the effect of drug after delivery and provide updated feedback on the phycological state of the body. Memory modules can be added to store and transfer data from continuous long-term monitoring which can then be used to reorganize patterns for disease progression and treatment. Moreover, rigid batteries can be replaced by compliant flexible and stretchable solar energy harvesting units such as solar cells in order to realize a fully conformal platform in the future.[35–37]

Experimental Section

The platform consisted of 3 different main layers. The heater layer, the expandable composite layer, and the microfluidics patch layer. The heater layer was fabricated electroplating 4 µm of copper on a on 25 µm thick polyimide film (Good Fellows). Prior to electroplating, the surface of polyimide substrate was treated with oxygen plasma to activate the surface and improve adhesion. After that and thing gold 150 nm layer was deposited using sputtering to act as a seed or adhesion layer for electroplating. After that, the sensors design/structures were pattern by laser ablation method using 1.06 µm ytterbium-doped fiber laser (PLS6MW Multi-Wavelength Laser Platform, Universal Laser Systems). The laser settings that were optimized for the pattering recipe were 30% power, 40% speed of the laser total capability. The expandable expancel polymer powder was purchased from Expancel, 031 DU 40, AkzoNobel in its powder form. The expandable layer was prepared by mixing expancel powder with mixed with polydimethylsiloxane (PDMS) (Sylgard 184 silicone elastomer kit) using a 2:1 ratio of PDMS to expancel in a vacuum mixer. The mixture was then spin coated on an empty wafer to fabricate a thin sheet of expandable polymer composite and cured in an oven at 70 °C for 2 h. The thin layer then can be peeled off the wafer carefully by using a razor blade to get a thin layer of 280 µm of expandable PDMS-expancel composite. This layer was then bonded on top of the heater layer using double sided adhesive film (30 µm thick, ARclear, Adhesive Research). The microfluidics layer was fabricated by 3D printing a master mold of the microfluidics layer (Figure S7a, Supporting Information). The printer that was used was Projet MJP 2500 plus sprinter (3D systems, USA) and rigid plastic white material VisiJet M2R-WT (MJP). The microfluidics chip structures of channels and reservoirs were designed using computer-aided design (CAD) software SolidWorks (2019), (Dassault Systèmes SE, France). The 3D CAD data were converted and sliced into layers and saved as. STL format, a format that compatible and widely used in most commercial 3D printers. After printing, the 3D master mold was cleaned using the Ease clean system of the printer to which consists of heated oil remove the structural wax supporting layers. After oil-bath cleaning,

additional cleaning steps were carried out by soaking the printed mold in soapy water and then into Isopropyl alcohol under sonication for 5 min. Afterwards, the mold was blow dried with nitrogen air and the 3D printed mold was treated with silicone ease- release spray to facilitate the demolding process later. PDMS mixture was prepared and casted on the master mold and inserted into a vacuum chamber for 20 min to remove any existing bubbles in the polymer. Later the PDMS was cured in the oven at 70 °C for 2 h. This layer then was bonded on top of the expandable composite layer using double sided adhesive film allowing direct contact between the expandable polymer and the reservoirs. The filling of reservoirs with liquid food dye colored was achieve using a fine needle and then the holes were sealed with transparent, water-proof tape (3M Corporation) and spin coating a thin layer of PDMS for total encapsulation. The inner surface of the microfluidics PDMS layer was coated with thin layer of parylene C (3 µm) to prevent fluid evaporation for long term storage. A hollow microneedle purchased from Micropoint Technologies was integrated into the microfluidics chip using small amount of clear epoxy resin. The microneedle was placed underneath the outlet at the end of the mixing structure. To complete the system, a driver circuitry was constructed to provide sufficient current for all heating elements to reach a certain temperature (above 80 °C). A 3.7 V lithium battery was used as the power unit and ATMEGA328 microcontroller was used as the processing unit. Fabricated flexible humidity and temperature sensor were used as well.

The experiments involving human subjects have been performed with the full, informed consent of the volunteers. Approval has been obtained from the KAUST Institutional Biosafety and Bioethics Committee (IBEC number 18IBEC16).

Supporting Information

Supporting Information is available from the Wiley Online Library or from the author.

Conflict of Interest

The authors declare no conflict of interest.

[1] M. A. Hamburg, F. S. Collins, *N. Engl. J. Med.* **2010**, *363*, 301.

[2] J. M. Nassar, M. D. Cordero, A. T. Kutbee, M. A. Karimi, G. A. T. Sevilla, A. M. Hussain, A. Shamim, M. M. Hussain, *Adv. Mater. Technol.* **2016**, *1*, 1600004.

[3] S. M. Khan, A. Gumus, J. M. Nassar, M. M. Hussain, *Adv. Mater.* **2018**, *30*, 1705759.

**ADVANCED
SCIENCE NEWS**

www.advancedsciencenews.com

**ADVANCED
MATERIALS
TECHNOLOGIES**

www.advmattechnol.de

[4] D. Liu, H. Zhang, F. Fontana, J. T. Hirvonen, H. A. Santos, *Lab Chip* **2017**, *17*, 1856.

[5] H. Lee, T. K. Choi, Y. B. Lee, H. R. Cho, R. Ghaffari, L. Wang, H. J. Choi, T. D. Chung, N. Lu, T. Hyeon, S. H. Choi, D. H. Kim, *Nat. Nanotechnol.* **2016**, *11*, 566.

[6] H. Kim, H. Lee, K. Y. Seong, E. Lee, S. Y. Yang, J. Yoon, *Adv. Healthcare Mater.* **2015**, *4*, 2071.

[7] J. Di, S. Yao, Y. Ye, Z. Cui, J. Yu, T. K. Ghosh, Y. Zhu, Z. Gu, *ACS Nano* **2015**, *9*, 9407.

[8] J.-W. Jeong, J. G. McCall, G. Shin, Y. Zhang, R. Al-Hasani, M. Kim, S. Li, J. Y. Sim, K.-I. Jang, Y. Shi, D. Y. Hong, Y. Liu, G. P. Schmitz, L. Xia, Z. He, P. Gamble, W. Z. Ray, Y. Huang, M. R. Bruchas, J. A. Rogers, *Cell* **2015**, *162*, 662.

[9] A. N. Damdam, N. Qaisar, M. M. Hussain, *Appl. Phys. Lett.* **2019**, *115*, 112105.

[10] A. Fry, *J. Diabetes Sci. Technol.* **2012**, *6*, 947.

[11] F. M White, *Viscous Fluid Flow*, McGraw-Hill, New York **1991**.

[12] C. Y. Lee, W. T. Wang, C. C. Liu, L. M. Fu, *Chem. Eng. J.* **2016**, *288*, 146.

[13] R. Karnik, F. Gu, P. Basto, C. Cannizzaro, L. Dean, W. Kyei-Manu, R. Langer, O. C. Farokhzad, *Nano Lett.* **2008**, *8*, 2906.

[14] L. M. Henricks, J. H. M. Schellens, A. D. R. Huitema, J. H. Beijnen, *Cancer Treat. Rev.* **2015**, *41*, 859.

[15] P. Karande, S. Mitragotri, *Biochim. Biophys. Acta, Biomembr.* **2009**, *1788*, 2362.

[16] B. Lin, *Microfluidics—Technologies and Applications*, 1st ed., Springer-Verlag, Berlin **2011**.

[17] G. S. Fiorini, D. T. Chiu, *BioTechniques* **2005**, *38*, 429.

[18] N. El-Atab, S. F. Shaikh, S. M. Khan, M. M. Hussain, *Adv. Eng. Mater.* **2019**, *21*, 1900043.

[19] J. Heikenfeld, A. Jajack, J. Rogers, P. Gutruf, L. Tian, T. Pan, R. Li, M. Khine, J. Kim, J. Wang, J. Kim, *Lab Chip* **2018**, *18*, 217.

[20] M. Teyssier, G. Bailly, C. Pelachaud, E. Lecolinet, A. Conn, A. Roudaut, in *Proc. 32nd Annual ACM Symp. on User Interface Software and Technology (UIST)*, New Orleans, LA, USA **2019**.

[21] A. Boonma, R. J. Narayan, Y. S. Lee, *Compu.-Aided Des. Appl.* **2013**, *10*, 139.

[22] A. M. Okamura, C. Simone, M. D. O'Leary, *IEEE Trans. Biomed. Eng.* **2004**, *51*, 1707.

[23] L. Filipovic, A. Lahlalia, *J. Electrochem. Soc.* **2018**, *165*, B862.

[24] S. Roy, C. K. Sarkar, *MEMS and Nanotechnology for Gas Sensors*, 1st ed., CRC Press, Boca Raton **2015**.

[25] W. J. Callahan, L. O. Narhi, A. A. Kosky, M. J. Treuheit, *Pharm. Res.* **2001**, *18*, 261.

[26] P. J. K. Steger, E. F. Martinelli, S. F. Mühlebach, *J. Clin. Pharm. Ther.* **1996**, *21*, 73.

[27] AkzoNobel, https://www.akzonobel.com/expancel/system/Images/A (accessed: March 2019).

[28] S. Spieth, *Ph.D. Thesis*, Albert-Ludwigs-Universität Freiburg im Breisgau, July **2013**.

[29] J. Cha, J. Kim, S. K. Ryu, J. Park, Y. Jeong, S. Park, S. Park, H. C. Kim, K. Chun, *J. Micromech. Microeng.* **2006**, *16*, 1778.

[30] C. C. Glick, M. T. Srimongkol, A. J. Schwartz, W. S. Zhuang, J. C. Lin, R. H. Warren, D. R. Tekell, P. A. Satamalee, L. Lin, *Microsyst. Nanoeng.* **2016**, *2*, 16063.

[31] L. Balasubramaniam, R. Arayanarakool, S. D. Marshall, B. Li, P. S. Lee, P. C. Y. Chen, *J. Micromech. Microeng.* **2017**, *27*, 095016.

[32] N. K. Adam, *Nature* **1940**, *146*, 145.

[33] E. C. Sweet, R. Mehta, Y. Xu, N. Liu, K. Korner, C. C. Glick, L. Lin, in *2019 20th Int. Conf. Solid-State Sensors, Actuators Microsystems Eurosensors XXXIII (TRANSDUCERS & EUROSENSORS XXXIII)*, Berlin, Germany, June **2019**.

[34] T. Pravinraj, R. Patrikar, *AIP Adv.* **2018**, *8*, 065112.

[35] N. El-Atab, W. Babatain, R. Bahabry, R. Alshanbari, R. Shamsuddin, M. M. Hussain, *ACS Appl. Mater. Interfaces* **2020**, *12*, 2269.

[36] N. El-Atab, N. Qaiser, R. Bahabry, M. M. Hussain, *Adv. Energy Mater.* **2019**, *9*, 1902883.

[37] R. R. Bahabry, A. T. Kutbee, S. M. Khan, A. C. Sepulveda, I. Wicaksono, M. Nour, N. Wehbe, A. S. Almislem, M. T. Ghoneim, G. A. Torres Sevilla, A. Syed, S. F. Shaikh, M. M. Hussain, *Adv. Energy Mater.* **2018**, *8*, 1702221.